J Solid State Electrochem (2010) 14:305–312
DOI 10.1007/s10008-009-0877-3

ORIGINAL PAPER

Synthesis, characterization and electrochemical behavior of the vanadium pentoxide/cetyl pyridinium chloride hybrid material

E. M. Guerra · D. T. Cestarolli · L. M. Da Silva · H. P. Oliveira

Received: 20 December 2008 / Revised: 26 May 2009 / Accepted: 29 May 2009 / Published online: 16 June 2009

Abstract In situ and ex situ studies concerning the new hybrid material vanadium pentoxide xerogel in the presence of the cationic surfactant cetyl pyridinium chloride (V_2O_5/CPC) are presented. The in situ characterization studies revealed the presence of a lamellar structure for the V_2O_5/CPC hybrid material. The intercalation reaction was evidenced on the basis of the increase in the *d*-spacing as well as the displacement of the infrared bands toward lower energy levels. Electrochemical studies comprising the cyclic voltammetry and the electrochemical impedance spectroscopy techniques showed that the behavior of the hybrid material is considerably influenced by the electrolyte composition. The ion insertion/de-insertion into the V_2O_5 xerogel structure accompanying the charge transfer process is influenced by the solid-state diffusion process modeled by using the finite-space Warburg element.

Keywords V_2O_5/cetyl pyridinium chloride · Surfactant · Hybrid material · Intercalation reaction · Electrochemical impedance spectroscopy

E. M. Guerra (✉) · H. P. Oliveira
Departamento de Química, Faculdade de Filosofia, Ciências e Letras de Ribeirão Preto, Universidade de São Paulo, Ribeirão Preto-SP, Brazil
e-mail: elidiamg@usp.br

D. T. Cestarolli
Universidade Federal de São João Del Rei, CAP, Ouro Branco-MG, Brazil

L. M. Da Silva
Departamento de Química/FACESA, Universidade Federal dos Vales do Jequitinhonha e Mucuri, Diamantina-MG, Brazil

Introduction

The vanadium pentoxide xerogel ($V_2O_5{\cdot}nH_2O$) is frequently employed as host material in intercalation reactions. It has been considered an important cathodic material for secondary lithium batteries for more than two decades [1], since it combines a layered structure suitable for insertion reaction with suitable electrochemical properties, not to mention its mixed ionic–electronic conductivity [2–6]. This particular interest, besides its the structural, ionic and electronic properties, is certainly enhanced by the fact that aqueous V_2O_5 gels are one of the best examples of materials synthesized through the "sol-gel process", which is capable of shaping and organizing the material guest via the "chimie douce" process, that is, soft chemistry [7]. The gel possesses a layered structure with an interlayer distance of 1.17 nm, and it is able to intercalate a variety of species [8]. The combination of organic and inorganic components can lead to $V_2O_5{\cdot}nH_2O$ with unusual properties, which might not be achieved with each component separately [9]. Improvement of the properties can be achieved by insertion of surfactants and polymeric materials as guests into the $V_2O_5{\cdot}nH_2O$ layers [4, 10, 11]. Oliveira *et al.* [12] have reported the electrochemical and conductivity properties obtained after insertion of melanin and polyaniline into the layers of $V_2O_5{\cdot}nH_2O$, which increased the dc conductivity and affected the spectroelectrochemical properties of the samples. However, the electrochemical behavior of the vanadium pentoxide xerogel intercalated with non-electoactive species, as surfactants, has been little explored [13]. Gimenes *et al.*[6] have reported on the synthesis and characterization of *N*-cetyl-*N*,*N*,*N*,-trimethyl-ammonim bromide (CTAB) into the V_2O_5, and they have studied the influence of surfactant molecules on its conductivity, electrochemical, and spectroelectrochemical properties

along with its potential application as a battery cathode. Silva *et al.* [14] have described the development of a modified electrode through the combination of the intrinsic conductivity property of the vanadium pentoxide xerogel with in the presence of the cationic surfactant CTAB following immobilization of electroactive anions such as hexacyanoferrate (III) and its analogue pentacyanonitrosylferrate (II). This study demonstrated that the CTAB inserted into the matrix caused an improvement in the difusional mobility because of the layer expansion caused by the presence of surfactant. Apart from the interlayer distance manipulation through insertion of the guest species insertion, the redox process, and the ion electroinsertion can lead to limitations, which depend on the ion present in the support electrolyte. Literature reports clearly demonstrate that the supporting electrolyte ions, M^+, play an important role in the electrode surface structure and can therefore affect electrode activity [15].

In this context, our interest is to prepare the V_2O_5/cetyl pyridinium chloride hybrid material (V_2O_5/CPC) and investigate the reversibility of the M^+ (Li^+, Na^+ and Et_4N^+) ion insertion/de-insertion into the V_2O_5 xerogel films resulting from the presence of CPC in the interlayer domain of the host structure. Moreover, we aimed at studying how the different ion sizes of the supporting electrolyte influence electrochemical properties, such as resistance, of the hybrid materials when this surfactant is inserted into the V_2O_5 interlayer.

Materials and methods

Reagents

All chemicals used in this work were reagent grade and were used without any previous treatment. Cetyl pyridinium chloride (98%) was purchased from Acros. Acetonitrile was chromatographic grade (Fluka).

Synthesis

The vanadium pentoxide gel, $V_2O_5{\cdot}nH_2O$, was prepared from sodium metavanadate ($NaVO_3$, 99%, Fluka) by the ion exchange method (ion-exchange resin Dowex-50X8). A decavanadic acid was obtained by percolating 0.10 mol L of a $NaVO_3$ aqueous solution through a cationic ion-exchange resin. Upon standing at room temperature (24 °C) for 2 weeks, the fresh HVO_3 solution was polymerized, leading to a viscous red V_2O_5 gel.

The V_2O_5/CPC hybrid material was prepared from the 20 mmol L of CPC added to 0.1 mol L V_2O_5 gel under constant stirring for 48 h. The resulting brown suspension was cast into a film form by evaporation of water at room temperature on a glass or another flat substrate (e.g. glassy carbon electrode). The resulting film was rinsed with deionized water and dried again at room temperature. The color of the film was light brown with a metallic luster.

Equipment and techniques

The X-ray diffraction (XRD) data were recorded on a SIEMENS D5005 diffractometer using a graphite monochromator and CuK_α emission line (1.541 Å, 40 kV, 40 mA). To this end, samples in the film form and deposited onto a glass plate were employed, and the data were collected at room temperature over the range $2^o \leq 2\theta \leq 50°$, with a step of 0.020°.

Fourier-transform infrared spectra (FTIR) were recorded from 4000 to 400 cm^{-1} on a Bomem MB 100 spectrometer. The samples were dispersed in KBr and pressed into pellets.

Scanning electron microscopy (SEM) was carried out on a ZEISS microscope EVO 50 model operating at 20 kV. A thin gold coating (≈ 20 Å) was applied to the sample using a Sputter Coater – Balzers SCD 050.

Cyclic voltammograms (CVs) and electrochemical impedance spectroscopy (EIS) spectra were measured using an AUTOLAB (EcoChemie - Netherlands) model PGSTAT30 (GPES/FRA) potentiostat/galvanostat interfaced with a computer. EIs spectra were recorded taking impedance measurements at specific potential values located in the charge transfer region. All impedance data were recorded using an a.c. perturbation signal of 5 mV (p/p), covering the 25 mHz – 100 kHz frequency range. The conventional electrode arrangement consisting of glassy carbon as supporting electrode, a platinum wire auxiliary electrode, and a saturated calomel reference electrode (SCE) was employed. The compounds were deposited onto the electrode surface by evaporating approximately 5 μL of the suspension at room temperature (24 °C). The supporting electrolytes were $LiClO_4$, $NaClO_4$, and Et_4NClO_4 in acetonitrile (1.0 mol L). The thickness of the film was approximately 4 μm and it was estimated using the optical fringe interference method [16, 17].

Results and discussion

Ex-situ characterization studies

Figure 1 depicts the X-ray diffraction patterns for the V_2O_5/CPC hybrid compound and for the vanadium pentoxide xerogel matrix. The diffractogram of the hybrid material (Fig. 1b) reveals the presence of narrow peaks, suggesting that this material has high crystallinity compared with the V_2O_5 xerogel matrix (Fig. 1a). Besides, the presence of the

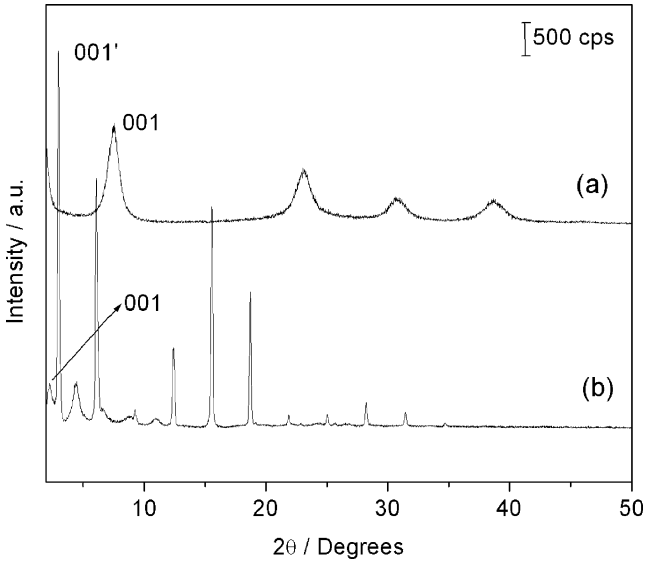

Fig. 1 X-ray diffraction patterns of the samples: (**a**) vanadium pentoxide xerogel and (**b**) V_2O_5/CPC

typical diffraction peaks (*001*) in the XRD patterns of the hybrid compound indicates a layered framework, showing that the lamellar structure of the V_2O_5 xerogel is maintained. In addition, after the insertion of CPC, it was possible to observe a shift of the 001 reflection to lower 2θ values, indicating that there is an increase in the interlayer spacing, which is consistent with the presence of the polymeric species in the matrix (*d*-spacing of 1.17 nm).

The increase in the interlayer distance was 3.92 nm, giving evidence of an intercalation reaction. Another important observation is that the 001 distance is much larger than the distance between the vanadium oxide planes in the crystalline powder or even when compared to $V_2O_5.1.6H_2O$ xerogels (d= 1.17 nm) [8]. According to the basal distance of 3.92 nm and taking the sheet thickness into account, one might suggest a configuration where the alkyl chains (d_{calc} ($C_{21}H_{38}ClNH_2$)=2.18 nm) are not tilted and form an angle of 90° with the oxide planes, while the hydrophilic chains are adsorbed onto vanadyl surface groups though hydrogen-bond interactions (see Scheme 1) [7].

All these points considered, the presence of the surfactant in the interlayer domain resulted in a perpendicular arrangement in the bilayer. Moreover, Fig. 1b shows that the presence of CPC promoted the formation of two phases or domain in the same intercalation compound (001 and 001′ diffraction peaks) [18]. This fact can indicate that the CPC molecules are reassembling in an intermittent way, consequently, giving rise to two domains.

Figure 2 shows the infrared spectra of the vanadium pentoxide xerogel matrix, CPC, and V_2O_5/CPC. The band at 1010 cm^{-1} has been ascribed to the V–O stretching of the vanadyl group (V=O), and the bands at 762 cm^{-1} and at 536 cm^{-1} are related to ν_{asym}(V–O–V) and ν_{sym}(V–O–V) vibration modes associated with the vanadium-oxide bridges, respectively [8, 11]. In the CPC spectrum, bands corresponding to ν(NH) - 3375 cm^{-1}; ν(CH) – 2840 cm^{-1};

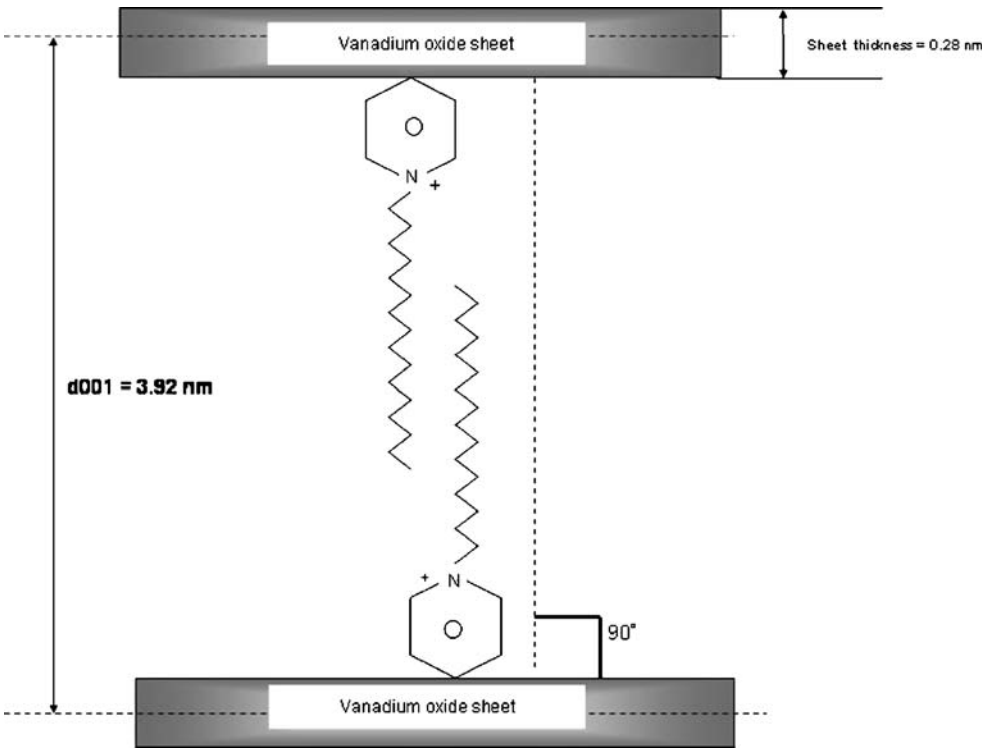

Scheme 1

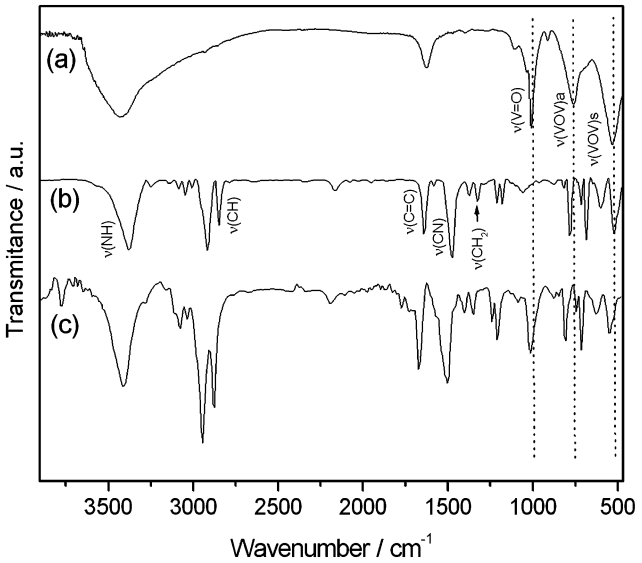

Fig. 2 FTIR spectra of the samples: (**a**) vanadium pentoxide xerogel, (**b**) CPC and (c) V_2O_5/CPC

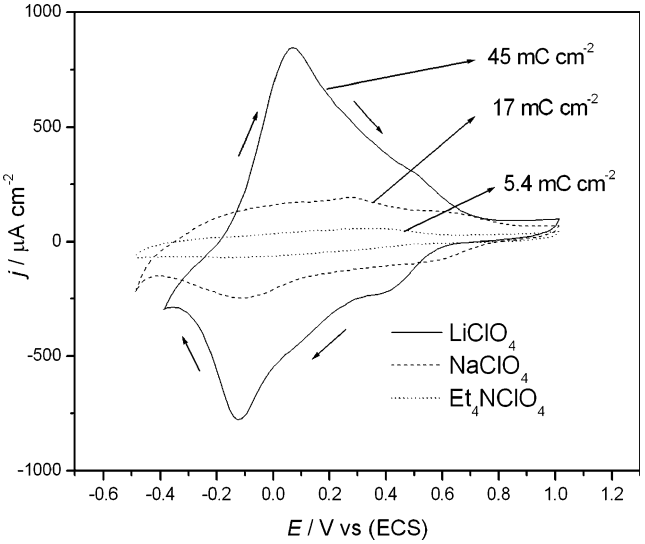

Fig. 4 Cyclic voltammograms of V_2O_5/CPC in acetonitrile containing (——) 0.1 M $LiClO_4$, (——) 0.1 M $NaClO_4$ and (·····) 0.1 M Et_4NClO_4, ν (20 mV s

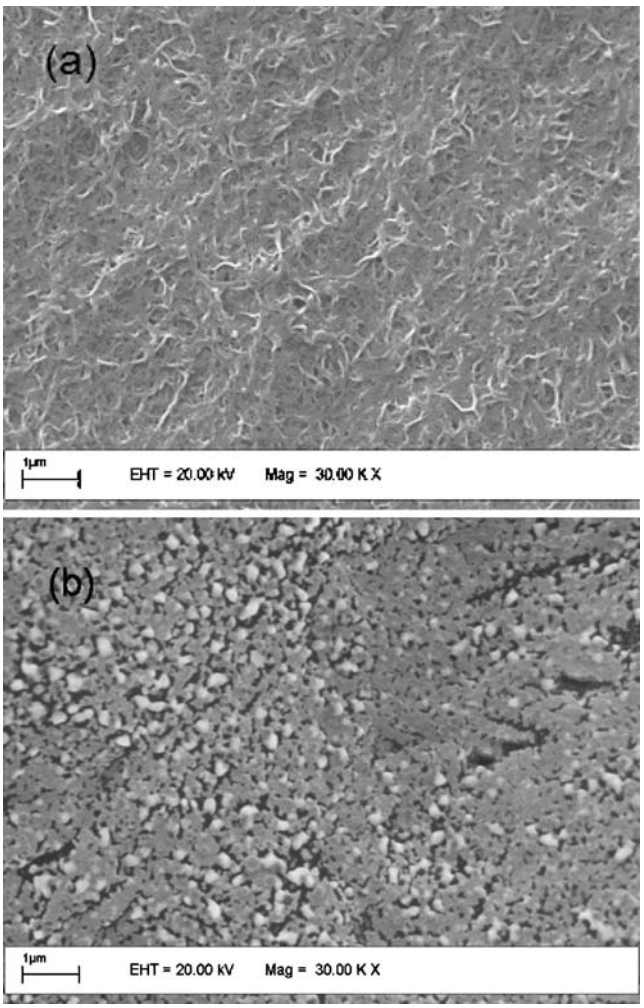

Fig. 3 Scanning electron micrographs of (**a**) vanadium pentoxide xerogel and (**b**) V_2O_5/CPC

ν(C=C) e ν(CN) - 1640 cm^{-1} e 1470 cm^{-1}, ν(CH_2) – 1320 cm^{-1} are observed [6]. After CPC insertion, there is a clear shift of the bands toward lower energy, corresponding to the V = O and V–O–V vibrational modes. These downshifts are probably due to electrostatic interactions between the positive charges of the surfactant in and the negative charge density of the V-O bond, which suggests a distortion of the coordination geometry at the metal centre. This probably arises from steric interactions between the confined surfactant and the V_2O_5 framework. Besides, according to Praus *et al.* [19], the CP^+ molecules of the hybrid compound are assumed to be attached to the matrix domain not only via the electrostatic forces but also through the induced interactions between aromatic pyridinium rings and negative charge density or hydrophobic π–π interactions of two neighboring pyridinium rings.

From the surface SEM image of the hydrated vanadium pentoxide matrix (Fig. 3a), one can observe the presence of interconnected agglomerates, fibrils, and ribbons, thus forming a network of chains. These agglomerates could be associated with nucleation centers [20]. The growth is promoted by oligomers in a first step and, in a second stage, the formation and growth of ribbons and fibrils take place, thereby promoting the organization of the polymeric chains in the $V_2O_5.nH_2O$. However, after the insertion of CPC, the

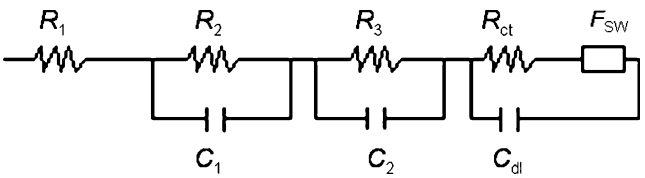

Fig. 5 Equivalent electrical circuit analogs based on the FSW element

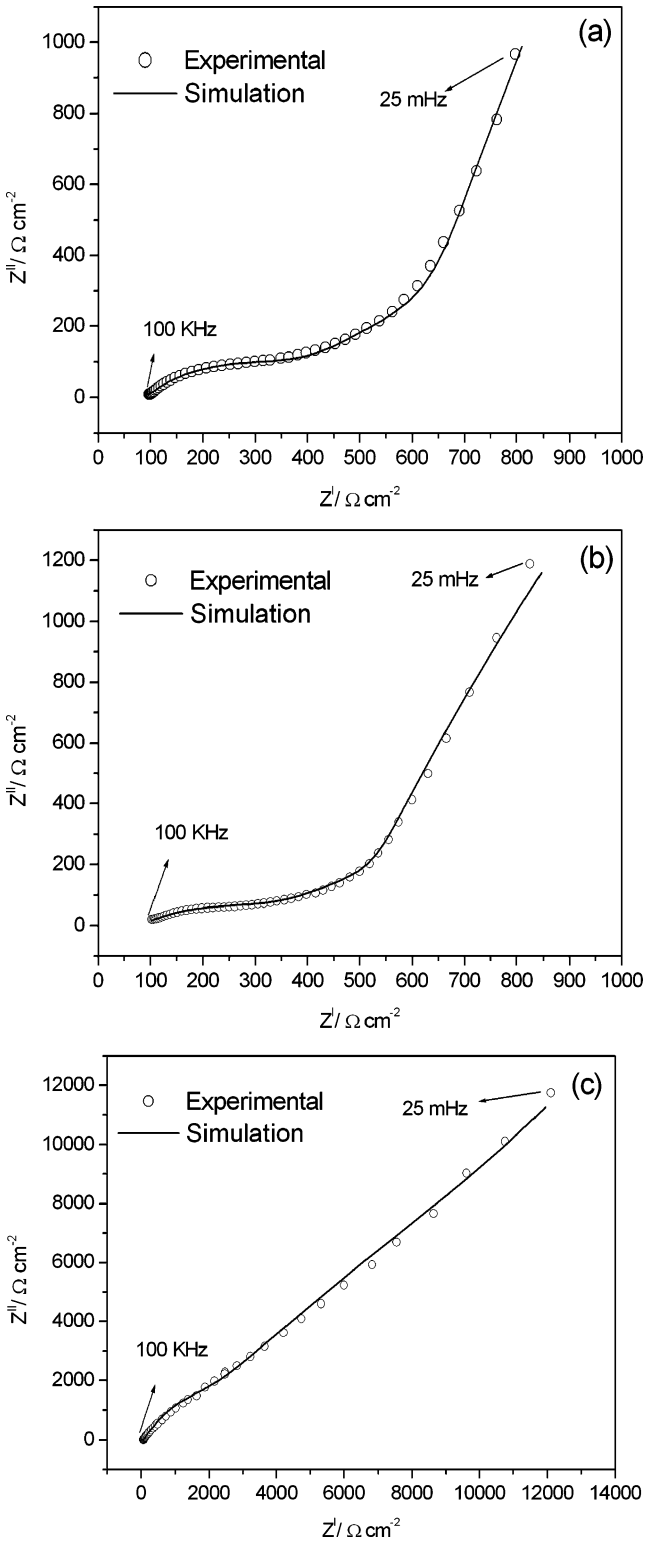

Fig. 6 Nyquist plot of the V_2O_5/CPC in acetonitrile containing (**a**) 0.1 M $LiClO_4$, (**b**) 0.1 M $NaClO_4$ and (**c**) 0.1 M Et_4NClO_4, during the transfer charge

SEM image (Fig. 3b) reveals changes in surface morphologies, with formation of an uneven and heterogeneous surface.

Electrochemical studies – CV and EIS

Cyclic voltammograms (CVs) of the V_2O_5/CPC hybrid compound are shown in Fig. 4. These cyclic voltammograms exhibit peaks in the potential range -0.50 V to +1.00 V (vs. SCE), in acetonitrile solution containing 0.1 mol dm^3 $MClO_4$ (which $M = Li^+$, Na^+ or Et_4N^+) attributed to the $V^{V/IV}$ redox pair with concomitant occurrence of M ion insertion and extraction ($xe^- + xM^+ + V_2O_5 \cdot nH_2O \leftrightarrows MxV_2O_5 \cdot nH_2O$) for maintenance of the charge balance.

Nevertheless, the cyclic voltammograms of the hybrid material display a change in the profile compared with the CV of the previously studied vanadium pentoxide xerogel [8]. This behavior can be associated with modifications in the structure after CPC insertion, which modify the electronic states of the conduction band and allow intercalation/deintercalation of more cations in different sites, compensating for the charge in the film [21]. In other words, the surfactant molecules cause a lamellar increase of the matrix, consequently, facilitating the access of the cations from the supporting electrolyte to the more internal sites. In addition, the use of different cations in the supporting electrolyte also resulted in an expressive change during the cyclic voltammetric. The presence of Li^+ ions during the insertion/de-insertion redox reaction provided well defined cathodic and anodic peaks compared with the cyclic voltammograms obtaining by using Na^+ and Et_4N^+ ions. This effect can be due to ion size and, as a consequence, the charge transfer occurs more easily for the Li^+ ions compared with the Na^+ and Et_4N^+ ions. As a result, it was possible to note that the total charges were 45, 17 and 5.4 mC cm^2 for Li^+, Na^+, and Et_4N^+, respectively. This total charge decrease demonstrates that the cation size can be directly related to the ion mobility through the film, and this fall arises from steric hindrance. Zanta *et al.* [15] reported that during the use of the Ti/RuO_2 e Ti/IrO_2 system there was a decrease in the current associated with ionic mobility through the electrode surface. These different results obtained by Zanta *et al.* demonstrated that the insertion of M^+ ions established the following sequence for the overall redox reaction: $Li^+ > Na^+ > Et_4N^+$.

It was found in the present study that the total charge decreasing and the electrochemical process concerning the ion intercalation are both influenced by the electrolyte composition; i.e., the size of the hydrated ion. Thus, we can argue that the cationic insertion process inside the host matrix is influenced by the rugged/porous morphology of the hybrid material. In the light of this consideration, the Et_4N^+ ion mainly reaches the more

Table 1 Optimized parameters obtaining using the CNLS fitting analysis. E=0.07 V (vs. Li^+), 0.29 V (vs. Na^+) and 0.41 V (vs. Et_4N^+). A_G= 0.5 cm^2

Material	$R_\Omega/\Omega\ cm^{-2}$	(τ_1)		(τ_2)		(τ_f)		FSW		
		$R_1/\Omega\ cm^{-2}$	$C_1/\mu F\ cm^{-2}$	$R_2/\Omega\ cm^{-2}$	$C_2/\mu F\ cm^{-2}$	$C_{dl}/\mu F\ cm^{-2}$	$R_{ct}/k\Omega\ cm^{-2}$	$R_{FSW}/\Omega\ cm^{-2}$	τ/s	α_{FSW}
V_2O_5/CPC (Li^+)	74.9	305.6	0.59	16.7	0.18	120	0.319	0.0015	8.9	0.43
V_2O_5/CPC (Na^+)	71.3	316.4	0.0064	7.11	$11x10^{-7}$	120	0.540	0.0051	8.5	0.44
V_2O_5/CPC (Et_4N^+)	67.7	266.2	0.35	85.1	68.2	47	0.981	0.0360	3.2	0.45

external region of the hybrid material (open pores/large cracks), while the Li^+ and Na^+ ions are able to reach more easily the internal structure of the film/solution interface (narrow pores/small cracks), thus resulting in a higher mobility in the lamellar space when compared with Et_4N^+.

Electrochemical impedance spectroscopy (EIS) studies were carried out in order to provide complementary and additional information concerning the influence of the ions present in the electrolyte $MClO_4$/ACN (M = Li, Na or Et_4N) on the electrochemical response accounted for the diffusion process taking place inside the film structure. The impedance response was modeled on the basis of the reflective boundary (finite length diffusion process), using the concept of the distributed elements [22].

Simulation of the experimental data was carried out via complex non-linear least square fitting analysis (CNLS) using a well-established equivalent circuit model (EC) proposed for the intercalation process [23–25].

The EC is mainly characterized by the short-time approximation to the finite-space diffusion using the finite space Warburg element (FSW) [22] (see Fig. 5). As previously reported by Mohamedi et al. [26], the diffusion element denoted as Z_{FSW} describes the diffusion process in non-isotropic medium where the porous/rugged interface precludes the flow of the species leading to the intercalation process.

According to the literature [23–28], the circuit elements presented in Fig. 5 can be identified as follow: R_Ω is the electrolyte resistance between the Luggin capillary and the working electrode; $\tau_1=R_1C_1$ and $\tau_2=R_2C_2$ are the time constants concerning the electrochemical behavior of the film/solution interface as functions of the penetration depth (the resistive-capacitive behavior associated with the slow ion migration from the external to the more internal regions of the hybrid material in the high-to-medium frequency domain); $\tau_f=R_{ct}C_{dl}$ is the time constant describing the charge transfer process, and Z_{FSW} is the resistance (impedance) imposed by the solid-state diffusion of ions inside the more compact regions of the intercalating material (e.g. narrow pores/deep cracks) in the medium-to-low frequency domain, whose impedance is denote as [24]:

$$Z_{FSW} = RL(j\omega\tau)^{-\alpha}\coth(j\omega\tau)^{\alpha}, \quad (1)$$

where: RL is the low-frequency limit of the real impedance (Z') and α is the adjustable parameter describing the non-ideal solid-state diffusion process in non-isotropic medium (α=0.5 for the ideal finite-space behavior).

Figure 6 shows the Nyquist plots obtained for the V_2O_5/CPC system in different electrolytes. Analysis of Fig. 6 reveals a rather good agreement between the EC model and the experimental impedance data obtained for low, medium, and high frequency domains. In all cases, the simulation procedure was characterized by chi-square, χ^2, values$<10^{-4}$.

Such findings are in good agreement with the literature [24, 26], where it was reported that simulation of the EIS data by electric analogs containing an FSW element is indeed appropriate to represent the impedance response of thin V_2O_5 electrodes. The reliability of the EIS technique for investigation of the intercalation process in non-isotropic oxide films was previously demonstrated by Levi et al. [28].

The optimized parameter values for the different elements present in EC were obtained using the EQUIVCRT program elaborated by Boukamp [29]. The result of the simulation procedure is presented in Table 1.

Analysis of Table 1 clearly reveals that R_1 is of the same order of magnitude. Considering that in all cases an average distance of 2 mm was kept between the working and the tip of the reference electrode, one can argue that both electrolytes present a similar ionic conduction in the electrolyte bulk. Analysis of the experimental data concerning the first and the second time constants (τ_1 and τ_2) reveals that the main change in the resistive behavior associated with the slow ion migration through the electrolyte/surface layer covering the active mass of the film is represented by the R_2 element: $R_2(Na^+) > R_2(Li^+) > R_2(Et_4N^+)$. In contrast, it was verified that $R_2(Na^+) \sim R_2(Li^+) < R_2(Et_4N^+)$ in the case of R_1.

Taking the physical meaning of the individual EC elements described in Fig. 5 into consideration, one can

argue that the resistive behavior presented by the ionic transport at the more-external surface regions of the active V_2O_5 film is more pronounced at the vicinity of the active bulk mass. Therefore, these findings indicate that ion penetration into the dense region of the active V_2O_5 film is considerable affected by the electrolyte composition (effective size of the solvated ion).

These findings are in agreement with the literature [30], where a linear relation between the degree of penetration of different ions into the more internal regions of the active metallic oxide coating and the thermochemical radii was reported.

The capacitance values evaluated via CNLS (see Table 1) are in good agreement with the literature [26], where was found capacitance values in the 0.7 to 47 mF cm^{-2} interval.

Impedance data analysis in the medium-to-low frequency domain revealed that the resistive/capacitive behavior is associated with the faradaic and the double layer charging process ($\tau_f=R_{ct}C_{dl}$), as shown by the fact that the Li-intercalation process is accompanied by lower resistance for the charge transfer process [24–27]. As for the intercalation of the Et_4N^+ ion, the R_{ct} value is considerably higher.

These findings are in agreement with the CV profiles (Fig. 4), where the pseudo-capacitive voltammetric charge related to the intercalation process follows the sequence: $q(Li^+) > q(Na^+) > q(Et_4N^+)$, thus revealing consistence between the experimental findings from different electrochemical techniques.

Analysis of Table 1 also shows that $R_{FSW}(Li^+) < R_{FSW}(Na^+) << R_{FSW}(Et_4N^+)$, thus indicating that the resistance associated with the mass diffusion process, which is experimentally evidenced by the medium frequency interval, is lower for the Li-intercalation process. As expected from the theoretical point of view, the high $R_{FSW}(Et_4N^+)$ value shows that the solid-state diffusion process taking place inside the V_2O_5 matrix (non-isotropic medium) decreases upon increase in the effective ionic-radius/charge ratio. Analysis of the time constant values associated with the diffusion process corroborates the previous discussion, thus revealing the important influence of the electrolyte nature on the electrochemical response of the V_2O_5 electrode system. Besides, the fact that $\alpha_{FSW}\cong 0.5$ shows that the solid-state diffusion process is well behaved.

Conclusion

Different ex-situ and in-situ studies were carried out in order to emphasize the dependence of the V_2O_5/CPC behavior on its composition and on the ionic species present in the electrolyte. The studies concerning the intercalation reaction with the vanadium pentoxide matrix and CPC showed that the lamellar structure of the matrix is preserved, but there is and an increase in crystallinity after CPC insertion. Additionally, the route employed in the preparation of V_2O_5 followed by intercalation with a surfactant material, leading to a hybrid material, was shown to be successful.

The electrochemical behavior of the hybrid material in presence of different electrolytes showed that the Et_4N^+ ion only reach the more external region (interface), while the Li^+ and Na^+ ions are able to penetrate into the more internal regions of the active layer located at the film/solution interface to a greater extent. Consequently, the lithium and sodium ions have more mobility compared with Et_4N^+ in the lamellar domain. A very good agreement was observed for the experimental findings from the CV and EIS techniques. The EIS analysis evidenced that the solid-state diffusion process taking place inside the V_2O_5 matrix decreases on increasing the effective ionic-radius/charge ratio, thus revealing the importance of the electrolyte composition on the electrochemical behavior of the intercalation process.

Acknowledgements The authors gratefully acknowledge the fellowship provided by CAPES, FAPESP and CNPq are also acknowledged for financial support.

References

1. Tipton AL, Passerini S, Owens BB, Smyrl WH (1996) J Electrochem Soc 143:3473
2. Lira-Cantu M, Gomez-Romero P (1999) J Electrochem Soc 144:2029
3. Huguenin F, Ferreira M, Zucolotto V, Nart FC, Torresi RM, Oliveira ON (2004) Chem Mater 16:2293
4. Posudievsky OY, Biskulova SA, Pokhodenko VD (2004) J Mater Chem 14:1419
5. Park NG, Ryu KS, Park YJ, Kang MG, Kim DK, Kang SG, Kim KM, Chang SH (2002) J Power Sources 103:273
6. Gimenes MA, Profeti LPR, Lassali TAF, Graeff CFO, Oliveira HP (2001) Langmuir 17:1975
7. Carn F, Steunou N, Livage J, Colin A, Backov R (2005) Chem Mater 17:644
8. Guerra EM, Ciuffi KJ, Oliveira HP (2006) J Solid State Chem 179:3814
9. Yano K, Usuki A, Okada A, Kurauchi T, Kamigaito O (1991) Polym Prepr 32:65
10. Ruckenstein E, Chao Z-S (2001) Nano Lett 1:739
11. Guerra EM, Brunello CA, Graeff CFO, Oliveira HP (2002) J Solid State Chem 168:134
12. Oliveira HP, Graeff CFO, Brunello CA, Guerra EM (2000) J Non-Crystalline Solids 273:193
13. Patrissi CJ, Martin CR (1999) J Electrochem Soc 146:3176
14. Silva LF, Profeti LPR, Stradiotto NR, Oliveira HP (2002) J Non-Crystalline Solids 298:213
15. Zanta CLPS, Andrade AR, Boodts JFC (1999) Electrochim Acta 44:3333
16. Li ZF, Ruckenstein E (2002) Langmuir 18:6956
17. Stine KE (1970) Beckman Infrared Laboratory Manual, Beckman Instruments Inc

18. Lindemuth PM, Bertrand GL (1993) J Phys Chem 97:7769
19. Praus P, Turicová M, Študentová S, Ritz M (2006) J Colloid Interface Sci 304:29
20. Guerra EM, Silva GR, Mulato M (2009) Solid State Sciences 11:456
21. Huguenin F, Giz MJ, Ticianelli EA, Torresi RM (2001) J Power Sources 103:113
22. Barsoukov E, Macdonald JR (2005) Impedance spectroscopy. John Wiley & Sons, Hoboken, New Jersey
23. Ho C, Raistrick ID, Huggins RA (1980) J Electrochem Soc 127:343
24. Levi MD, Lu Z, Aurbach D (2001) Solid State Ionics 143:309
25. Levi MD, Aurbach D (2005) J Power Sources 146:349
26. Mohamedi M, Takahashi D, Uchiyama T, Itoh T, Nishizawa M, Uchida I (2001) J Power Sources 93:93
27. Thomas MGSR, Bruce PG, Goodenough JB (1985) J Electrochem Soc 132:1521
28. Levi MD, Lu Z, Aurbach D (2001) J Power Sources 97–98:482
29. Boukamp BA (1986) Solid State Ionics 20:31
30. Da Silva LM, Faria LA, Boodts JFC (2001) Electrochim Acta 47:395